Supplementary Information for

Dynamically Structured Bubbling in Vibrated Gas-Fluidized Granular Materials

Qiang Guo[a], Yuxuan Zhang[a], Azin Padash[a], Kenan Xi[a,b],
Thomas M. Kovar[a], Christopher M. Boyce[a,1]

[a]Department of Chemical Engineering, Columbia University, New York, NY 10027, USA
[b]State Key Laboratory of Multiphase Flow in Power Engineering, Xi'an Jiaotong University, Xi'an 710049, China

[1]Corresponding Author. Email: cmb2302@columbia.edu

Experiments

Fig. 1 shows a schematic of the experimental setup. Most of the experiments were conducted in a fluidized bed 200 mm in width, 500 mm in height and 10 mm in depth. Some experiments shown in Fig. 4*C*, Fig S2 and Table S1 were also conducted in an identical system, but with a width of 400 mm. For each experiment, images were taken at a frame rate of 50 images per second for 3 minutes after the fluidization behavior reached a steady state, producing a total of 9,000 frames. These 9,000 frames were divided into 9 segments, each consisting of 1,000 frames. For each frame, the correlation coefficient and the number-averaged bubble diameter (D_b), bubble rise velocity (u_b), horizontal bubble distance (λ_H) and vertical bubble distance (λ_V) as well as their standard deviation were calculated. Then, for each segment, the averaged value of a certain property was obtained as the average over all the 1000 frames. The average and standard deviation of the averaged values obtained in these 9 segments were then obtained and finally shown in Fig. 3 *A*, *B* and *C*, Fig. 4 *B* and *C*, Fig. S1, Fig. S2, Table 1 and Table S1.

Fig. S1 shows the average bubble diameter (D_b, first row) and standard deviation of bubble diameter normalized by average bubble diameter (σ_{Db}/D_b, second row) versus (*A*) vibration frequency, (*B*) vibration amplitude and (*C*) U/U_{mf}.

Fig. S2 shows correlation coefficient versus (*A*) vibration frequency, (*B*) vibration amplitude and (*C*) U/U_{mf} for a bed 40 cm in width.

Table S1 compares bubble properties under optimal flow and vibration conditions for the 20 cm wide bed and the 40 cm wide bed.

Fig. S4 shows the optical images of bubbles in silicone oil during two vibration cycles. The initial silicone oil height is 10 cm. The vibration frequency is 5 Hz and the vibration amplitude is 4.5 mm. The superficial gas velocity is 1.17 cm/s. The silicone oil was ordered from Clearco

Products Co., Inc. The dynamic viscosity of the silicone oil is 1.0 Pa s. The experiments associated with the silicone oil were run using the same experimental setup used for fluidized particles.

Discrete particle simulations

The discrete particle simulations were conducted using CFD-DEM (Computational Fluid Dynamics – Discrete Element Method) with the open-source platform CFDEMcoupling (1). The simulations were conducted in a fluidized bed of 100 mm in width, 100 mm in height and 2 mm in depth. The modeled fluid phase had a viscosity of 1.8×10^{-5} Pa s and a density of 1.2 kg/m^3, similar to the properties of air at atmospheric pressure. The fluidized particles were spherical in shape with the size of 238 μm and density of 2500 kg/m^3, similar to the glass beads used in experiments with the size of 212-300 μm and the density of 2500 kg/m^3. The initial bed height was 55 mm. The fluid grid size was 1 mm (horizontal) by 1 mm (vertical) by 1 mm (depth), approximately 4 particle diameters in side length. Instead of physically moving the bottom plate, vibration was modeled by oscillating the gravitational force (2) with a frequency of 5 Hz and an amplitude of 8 mm. Gravitational acceleration was oscillated according to: $g = 4\pi^2 f^2 A sin(2\pi f t) + 9.81$, where f is the frequency of vibration and A is the amplitude of vibration (correspond in the experimentally vibrated system to the height of the bottom plate at its highest point minus its height at its midpoint in vibration) with units of length. The inlet boundary condition was set to a constant superficial gas velocity (U) with U/U_{mf} = 1.39. The outlet boundary condition was constant atmospheric pressure. The walls along the width direction were set as periodic boundaries, while the walls along the depth direction were set as rigid walls for particles and no-slip boundary conditions for the gas phase. The U_{mf} was determined by slowly decreasing U and monitoring the bed pressure drop. The coupling between gas and particles was accounted for using the Gidaspow drag law (3). The simulations were run for 10 s with a time step of $2 \times 10^{-}$

^{6} s for particles and a time step of 1×10^{-4} s for the gas phase. Detailed parameters are summarized in Table S2.

The particle position, local solids volume fraction and particle contact force normalized by particle weight were output to create Fig. 5 and Fig. S3. The solids pressure produced in discrete particle simulations, as shown in Fig. 6*D*, was based on the computationally generated constitutive models proposed by Gu et al. (4).

Fig. S3 shows the particle contact force normalized by particle weight during two vibration cycles obtained from discrete particle simulations.

Continuum simulations

Fully continuum simulations were conducted using MFiX (5), which already had two predominantly used frictional solids stress models built into it: the Schaeffer model (6) and the Srivastava and Sundaresan model (7). We built the proposed model detailed below into MFiX as a user-defined function.

Model equations

As discussed in the main document, we proposed a critical state solids pressure formulation shown in Eq. **11**. We use this formulation to replace the Srivastava and Sundaresan model (7) formulation when the solids concentration is between $\varepsilon_{s,minf}$ and $(\varepsilon_{s,max} - \delta)$, where δ is a constant with a small value. This formulation, however, shows inherent discontinuity when the solids concentration equals either $\varepsilon_{s,minf}$ or $(\varepsilon_{s,max} - \delta)$. To solve this, additional terms are adopted. In particular, a transition factor $t_1 = \frac{2\times\arctan[10^4\times(\varepsilon_s - \varepsilon_{s,minf})]}{\pi}$ that changes from 0 to 1 rapidly when ε_s is increasing from $\varepsilon_{s,minf}$ to a value slightly larger than $\varepsilon_{s,minf}$ is multiplied by $\frac{((\varepsilon_{s,max} - \varepsilon_{s,minf})\dot{\gamma} d_p)^2 \rho_p}{(\varepsilon_{s,max} - \varepsilon_s)^2}$ to calculate p_c in the intermediate regime. Further, the formulation in the

Schaeffer model (6) is added to $\frac{\left((\varepsilon_{s,max}-\varepsilon_{s,minf})\dot{\gamma}d_p\right)^2\rho_p}{\delta^2}$ when $\varepsilon_s > (\varepsilon_{s,max}-\delta)$, to calculate p_c in the frictional regime to prevent over-packing of the solids phase. We ultimately formulate an equation for critical solids pressure, shown in Eq. **S1**.

$$p_c = \begin{cases} \frac{\left((\varepsilon_{s,max}-\varepsilon_{s,minf})\dot{\gamma}d_p\right)^2\rho_p}{\delta^2} + A_{pc}\left(\varepsilon_s+\delta-\varepsilon_{s,max}\right)^{n_{pc}} & \varepsilon_s > (\varepsilon_{s,max}-\delta) \\ t_1\frac{\left((\varepsilon_{s,max}-\varepsilon_{s,minf})\dot{\gamma}d_p\right)^2\rho_p}{\left(\varepsilon_{s,max}-\varepsilon_s\right)^2} & \varepsilon_{s,minf} \le \varepsilon_s \le (\varepsilon_{s,max}-\delta) \\ 0 & \varepsilon_s < \varepsilon_{s,minf} \end{cases} \quad \text{(S1)}$$

where A_{pc} and n_{pc} are two constants used in the Schaeffer model (6).

All other equations for solids stress are kept the same as in the Srivastava and Sundaresan model (7). The relationship between the frictional solids pressure p_s^f and p_c is

$$\frac{p_s^f}{p_c} = \left[1-\frac{\nabla\cdot\vec{u}_s}{n\sqrt{2}\sin(\phi)\sqrt{\boldsymbol{S}:\boldsymbol{S}+\Theta_s/d_p^2}}\right]^{n-1} \quad \text{(S2)}$$

where ϕ is the angle of internal friction, $\boldsymbol{S}$ is the deviatoric rate-of-strain tensor, $\vec{u}_s$ is the solids phase velocity and Θ_s is the granular temperature. The exponent n in Eq. **S2** has different values depending on whether the granular assembly is dilating or compacting.

$$n = \begin{cases} \frac{\sqrt{3}}{2\sin(\phi)} & \nabla\cdot\vec{u}_s \ge 0 \\ 1.03 & \nabla\cdot\vec{u}_s < 0 \end{cases} \quad \text{(S3)}$$

The solids viscosity is calculated using

$$\mu_s^f = \frac{\sqrt{2}p_s^f\sin(\phi)}{2\sqrt{\boldsymbol{S}:\boldsymbol{S}+\Theta_s/d_p^2}}\left[n-(n-1)\left(\frac{p_s^f}{p_c}\right)^{\frac{1}{n-1}}\right] \quad \text{(S4)}$$

Compared to the Srivastava and Sundaresan model (7), the proposed model only changes the formulation of p_c, yet this formula affects both the solids pressure and solids viscosity.

Table S3 lists the values of the constants used in different models, based on values commonly used in the literature (6, 7).

Simulation details

The continuum simulations were conducted in a fluidized bed of 200 mm in width, 160 mm in height and 2 mm in depth. The grid size, gas viscosity and density, particle size and density, boundary condition type, drag law model and restitution coefficient used in the continuum simulations were the same as in the discrete particle simulations. To avoid divergence problems, initially, the solids phase with the volume fraction of 0.55 was loaded into the bed at a height of 106 mm. Vibration was accounted for by oscillating gravity, as done in the discrete particle simulations, but with a frequency of 5 Hz and an amplitude of 4.5 mm. To close the kinetic solids pressure and solids viscosity, the kinetic theory of Lun et al. (8) was used. Frictional solids stress was accounted for by either using the Schaeffer model (6), the Srivastava and Sundaresan model (7) or the proposed model. The simulations were run for 10 s with a time step of 1×10^{-4} s. Detailed parameters are summarized in Table S4.

The local solids volume fraction and solids pressure produced in the continuum simulations were output to create Fig. 6 *A*, *B*, *C*, *E*, and *F*, Fig. S5 and Fig. S6. The input parameters used to make Fig. 6*G* were extracted from the typical parameter values observed in simulations: $\dot{\gamma}$ = 65 s^{-1}, $\Theta_s = 1 \times 10^{-4}$ m^2/s^2, n = 1.03, $\nabla \cdot \vec{u}_s$ = -10 s^{-1}, ρ_p = 2500 kg/m^3 and d_p = 238 μm.

Fig. S5 shows the snapshots of local solids volume fraction during two vibration cycles predicted by the continuum simulations using (*A*) the Schaeffer model (6), (*B*) the Srivastava and Sundaresan model (7) and (*C*) our proposed model.

Fig. S6 shows the snapshots of local solids volume fraction during two gas flow oscillation cycles predicted by the continuum simulations using (*A*) the Schaeffer model (6), (*B*) the Srivastava and Sundaresan model (7) and (*C*) our proposed model.

Video Legends:

The SI Video includes optical imaging experiments as well as discrete particle simulations and fully continuum simulations of the structured bubbling reported in this paper.

References

1. C. Kloss, C. Goniva, A. Hager, S. Amberger, S. Pirker, Models, algorithms and validation for opensource DEM and CFD–DEM. *Prog. Comput. Fluid Dyn. Int. J.* **12**, 140–152 (2012).

2. C. P. McLaren, T. M. Kovar, A. Penn, C. R. Muller, C. M. Boyce, Gravitational instabilities in binary granular materials. *Proc. Natl. Acad. Sci.* **116**, 9263–9268 (2019).

3. J. Ding, D. Gidaspow, A bubbling fluidization model using kinetic theory of granular flow. *AIChE J.* **36**, 523–538 (1990).

4. Y. Gu, A. Ozel, J. Kolehmainen, S. Sundaresan, Computationally generated constitutive models for particle phase rheology in gas-fluidized suspensions. *J. Fluid Mech.* **860**, 318–349 (2019).

5. J. M. Musser, J. E. Carney, "Theoretical Review of the MFIX Fluid and Two-Fluid Models" *DOE/NETL Technical Report* (2020).

6. M. Syamlal, W. Rogers, T. J. O`Brien, "MFIX documentation theory guide" *DOE Technical Note* (1993).

7. A. Srivastava, S. Sundaresan, Analysis of a frictional–kinetic model for gas–particle flow. *Powder Technol.* **129**, 72–85 (2003).

8. C. K. K. Lun, S. B. Savage, D. J. Jeffrey, N. Chepurniy, Kinetic theories for granular flow: inelastic particles in Couette flow and slightly inelastic particles in a general flowfield. *J. Fluid Mech.* **140**, 223–256 (1984).

Tables

Table S1. Comparison of bubble properties at resonant conditions in beds with different widths

Particle type	Particle size (μm)	Particle density (kg/m^3)	20 cm width bed				40 cm width bed			
			D_b (mm)	u_b (m/s)	λ_H (mm)	λ_V (mm)	D_b (mm)	u_b (m/s)	λ_H (mm)	λ_V (mm)
Glass beads	212-300	2500	20±3	0.31±0.04	66±12	60±7	19±4	0.30±0.05	67±14	60±8
Glass beads	400-600	2500	20±5	0.30±0.06	64±15	58±8	20±6	0.30±0.06	64±16	57±9

Table S2. Detailed parameters used in the discrete particle simulations

Quantity	Symbol	Unit	Value
Geometry (Width × depth × height)	$L_x \times L_y \times L_z$	mm	100 × 2 × 100
Number of CFD cells	$N_x \times N_y \times N_z$	-	100 × 2 × 100
Gas density	ρ_g	kg/m^3	1.2
Gas viscosity	μ_g	Pa·s	1.8×10^{-5}
Number of particles	N_p	-	949,458
Initial particle height (m)	H_B	mm	55
Particle diameter	d_p	μm	238
Particle density	ρ_p	kg/m^3	2500
Friction coefficient	μ	-	0.35
Restitution coefficient	e	-	0.97
Poisson's ratio	ϑ	-	0.22
Young's modulus	E	Pa	1×10^6
Vibration frequency	f	Hz	5
Vibration amplitude	A	mm	8
Drag law model	-	-	Gidaspow
CFD inlet boundary condition	-	-	Fixed Velocity
CFD outlet boundary condition	-	-	Atmospheric pressure
Wall boundary condition	-	-	Periodical in the *x* direction No-slip in the *y* direction
CFD time step	dt_{CFD}	s	1×10^{-4}
DEM time step	dt_{DEM}	s	2×10^{-6}
Gravitational acceleration	$\vec{g}$	m/s^2	$9.81 + (2\pi f)^2 A sin(2\pi f t)$

Table S3. Typical values of the constants used in the continuum simulations

Parameter	$\varepsilon_{s,max}$	$\varepsilon_{s,minf}$	A_{pc}	n_{pc}	δ
Value	0.63	0.5	10^{24}	10	0.01

Table S4. Detailed parameters used in the continuum simulations

Quantity	Symbol	Unit	Value
Geometry (Width × depth × height)	$L_x \times L_y \times L_z$	mm	200 × 2 × 160
Number of CFD cells	$N_x \times N_y \times N_z$	-	200 × 2 × 160
Gas density	ρ_g	kg/m^3	1.2
Gas viscosity	μ_g	Pa·s	1.8×10^{-5}
Initial bed height (m)	H_B	mm	106
Initial packing concentration	$\varepsilon_{s,init}$	-	0.55
Solids size	d_p	μm	238
Solids density	ρ_p	kg/m^3	2500
Restitution coefficient	e	-	0.97
Angle of internal friction	ϕ	°	28.5
Angle of wall friction	ϕ_w	°	12.3
Vibration frequency	f	Hz	5
Vibration amplitude	A	mm	4.5
Drag law model	-	-	Gidaspow
Viscous stress model	-	-	Lun et al.
Frictional stress model	-	-	Schaeffer model, Srivastava and Sundaresan model, or the proposed model
Inlet boundary condition	-	-	Fixed velocity
Outlet boundary condition	-	-	Atmospheric pressure
Wall boundary condition	-	-	Periodical in the *x* direction No-slip in the *y* direction
Time step	dt_{CFD}	s	1×10^{-4}
Gravitational acceleration	$\vec{g}$	m/s^2	$9.81 + (2\pi f)^2 A sin(2\pi f t)$

Figures

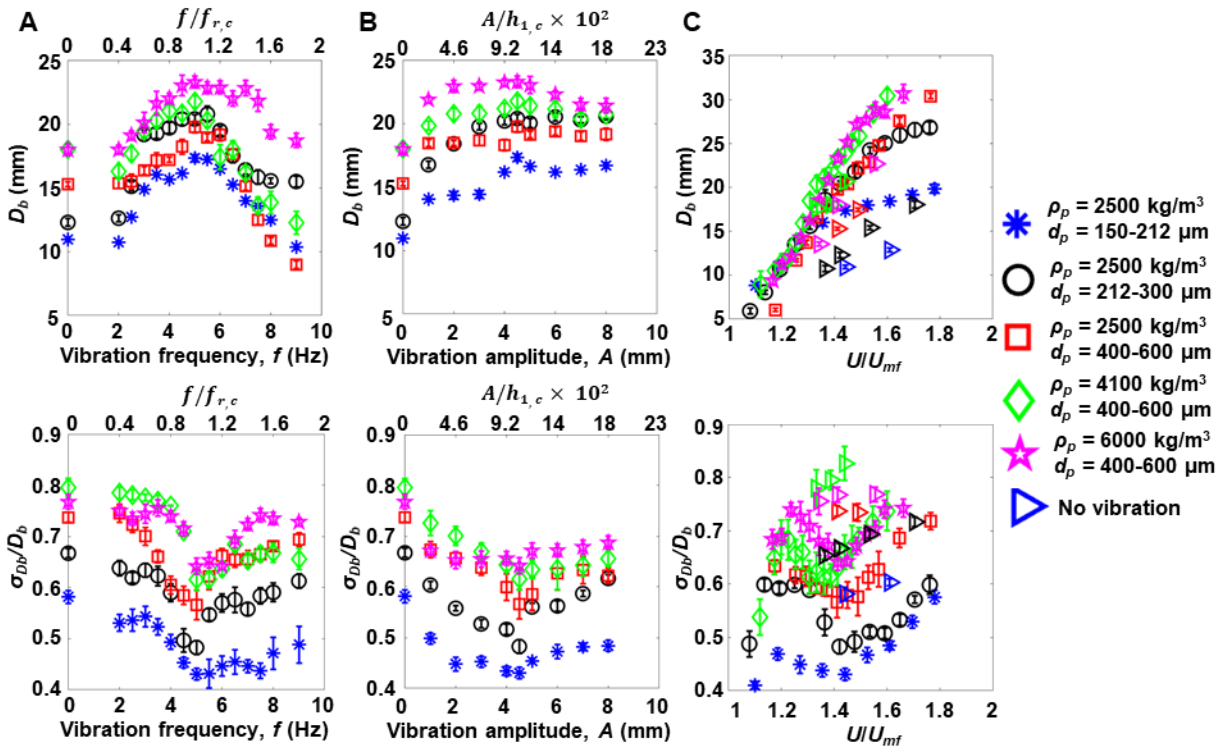

Fig. S1. Average bubble diameter (D_b, first row) and standard deviation of bubble diameter normalized by average bubble diameter (σ_{Db}/D_b, second row) versus (*A*) vibration frequency, (*B*) vibration amplitude and (*C*) U/U_{mf}. Each panel of images varies a property while keeping other properties constant: (*A*) Constant properties: vibration amplitude = 4.5 mm, U/U_{mf} = 1.4. (*B*) Constant properties: vibration frequency = 5 Hz, U/U_{mf} = 1.4. (*C*) Constant properties: vibration frequency = 5 Hz, vibration amplitude = 4.5 mm. The initial particle height is 10 cm in (*A*-*C*). The right-pointing triangles in (*C*) denote experiments without system vibration.

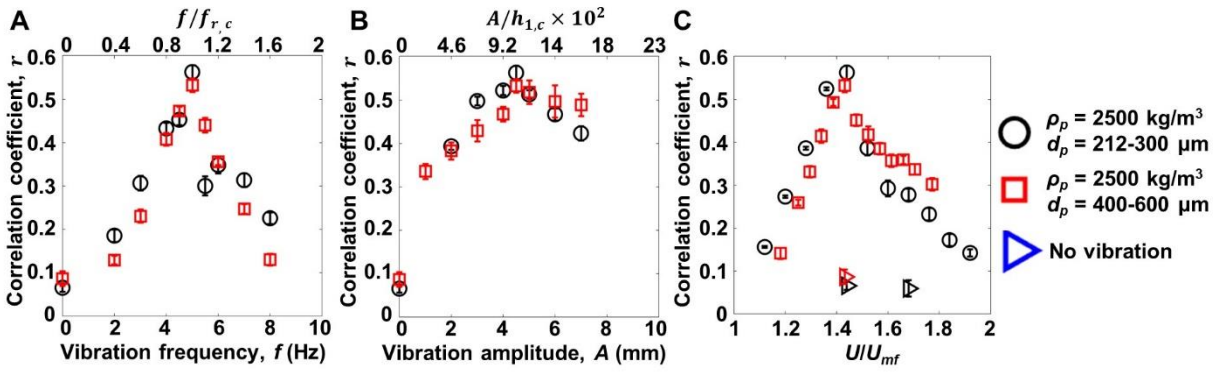

Fig. S2. Vibration and flow conditions needed to produce structured bubbling in the bed with 40 cm width: Correlation coefficient versus (*A*) vibration frequency, (*B*) vibration amplitude and (*C*) U/U_{mf}. Each panel of images varies a property while keeping other properties constant: (*A*) Constant properties: vibration amplitude = 4.5 mm, U/U_{mf} = 1.4. (*B*) Constant properties: vibration frequency = 5 Hz, U/U_{mf} = 1.4. (*C*) Constant properties: vibration frequency = 5 Hz, vibration amplitude = 4.5 mm. The initial bed height is 10 cm in (*A*-*C*). The right-pointing triangles in (*C*) denote experiments without system vibration.

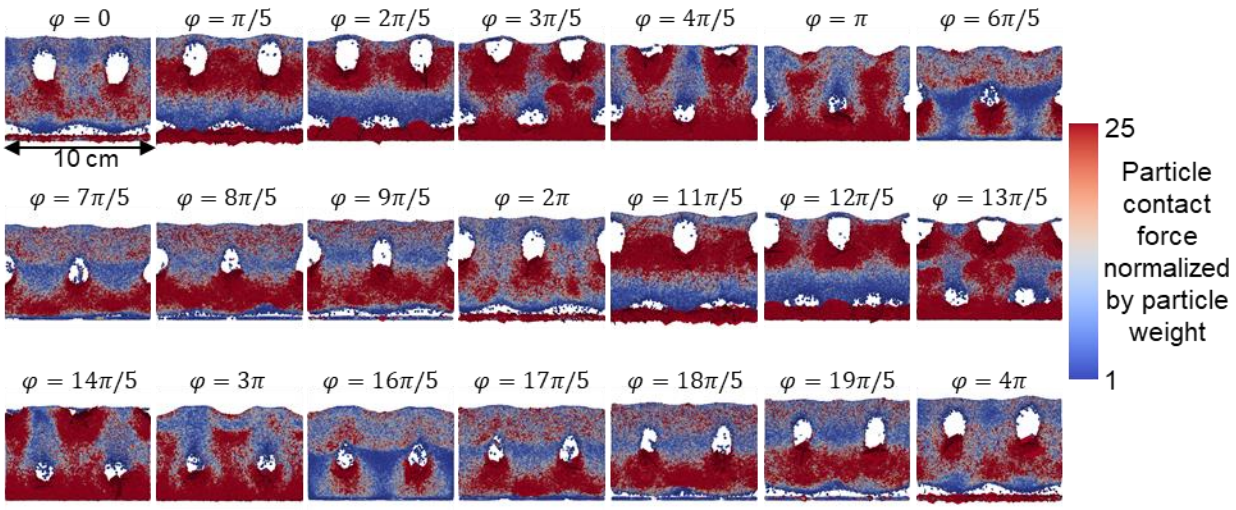

Fig. S3. Particle contact force normalized by particle weight during two vibration cycles obtained from discrete particle simulations. The simulated particles have properties ρ_p = 2500 kg/m^3 and d_p = 238 μm. The vibration frequency and amplitude are 5 Hz and 8 mm, respectively. The U/U_{mf} is 1.39.

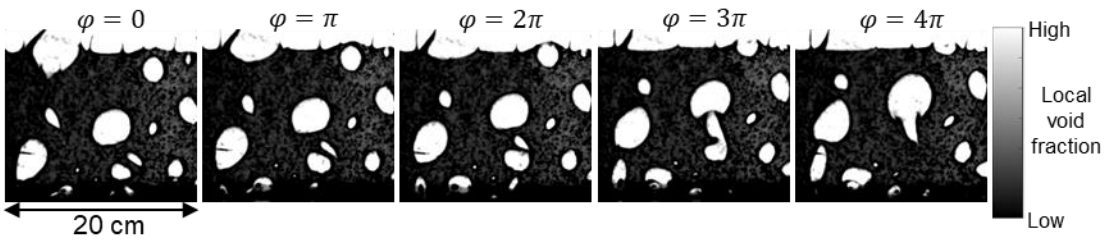

Fig. S4. Optical images of bubbling pattern in silicone oil during two vibration cycles. The initial silicone oil height is 10 cm. The dynamic viscosity of the silicone oil is 1.0 Pa s. The vibration frequency is 5 Hz and the vibration amplitude is 4.5 mm. The superficial gas velocity is 1.17 cm/s.

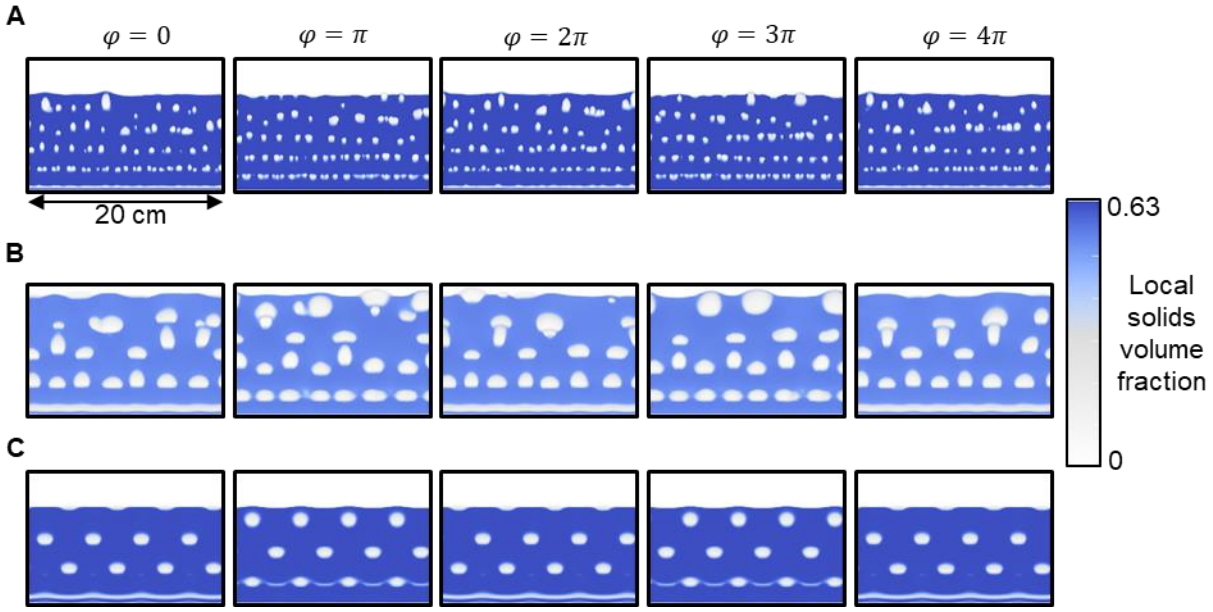

Fig. S5. Snapshots of local solids volume fraction during two vibration cycles predicted by continuum gas-solid flow modeling using different constitutive models: (*A*) Schaeffer model (6), (*B*) Srivastava and Sundaresan model (7) and (*C*) the proposed model. The simulated solids phase has properties ρ_p = 2500 kg/m^3 and d_p = 238 μm. The vibration frequency and amplitude are 5 Hz and 4.5 mm, respectively. The U/U_{mf} is 1.37.

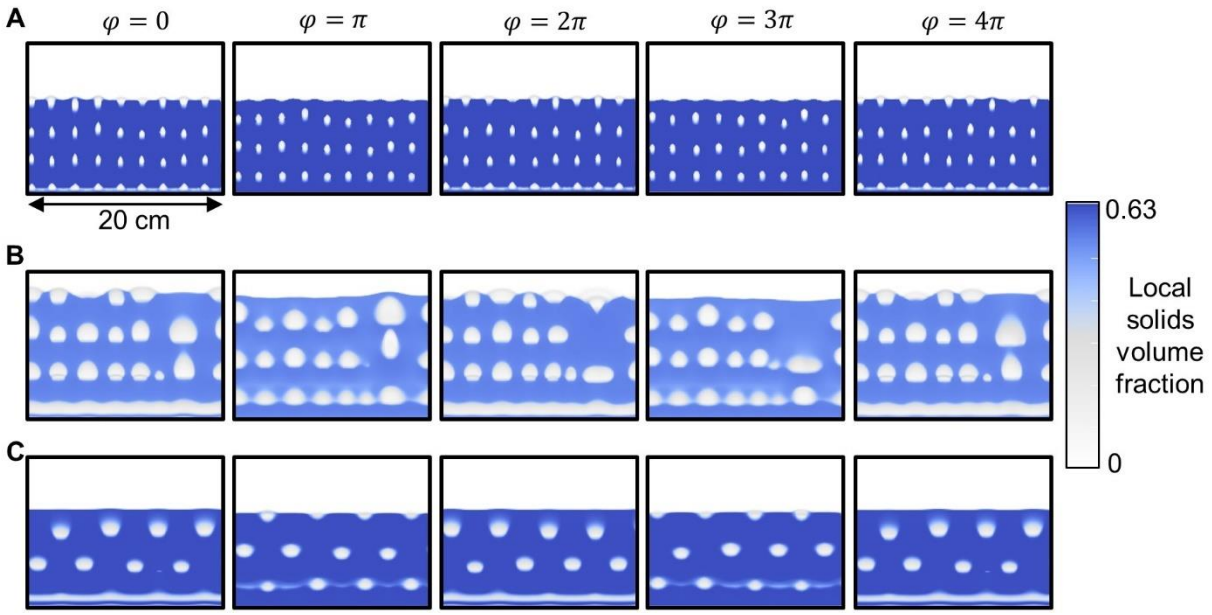

Fig. S6. Snapshots of local solids volume fraction during two gas flow oscillation cycles predicted by continuum gas-solid flow modeling using different constitutive models: (*A*) Schaeffer model (6), (*B*) Srivastava and Sundaresan model (7) and (*C*) the proposed model. The simulated solids phase has properties ρ_p = 2500 kg/m^3 and d_p = 238 μm. The average normalized gas velocity is U_{avg}/U_{mf} = 1.54; the amplitude of gas flow oscillation is U_{amp}/U_{mf} = 1.25; the frequency of gas flow oscillation is 5 Hz; the equation for superficial gas velocity is $U = U_{avg} - U_{amp}\sin(2\pi f t)$.